Stem Cell Reports
Resource
ISSCR
OPEN ACCESS

Agarose microgel culture delineates lumenogenesis in naive and primed human pluripotent stem cells

Magdalena Schindler,[1,2,3,5] Dylan Siriwardena,[1,2,3,5] Timo N. Kohler,[3,4,5] Anna L. Ellermann,[4] Erin Slatery,[1,2,3] Clara Munger,[1,2,3] Florian Hollfelder,[4,*] and Thorsten E. Boroviak[1,2,3,*]

[1]Department of Physiology, Development and Neuroscience, University of Cambridge, Downing Site, Cambridge CB2 3EG, UK
[2]Centre for Trophoblast Research, University of Cambridge, Downing Site, Cambridge CB2 3EG, UK
[3]Wellcome Trust – Medical Research Council Stem Cell Institute, University of Cambridge, Jeffrey Cheah Biomedical Centre, Puddicombe Way, Cambridge CB2 0AW, UK
[4]Department of Biochemistry, University of Cambridge, 80 Tennis Court Road, Cambridge CB2 1GA, UK
[5]These authors contributed equally
*Correspondence: fh111@cam.ac.uk (F.H.), teb45@cam.ac.uk (T.E.B.)
https://doi.org/10.1016/j.stemcr.2021.04.009

SUMMARY

Human periimplantation development requires the transformation of the naive pluripotent epiblast into a polarized epithelium. Lumenogenesis plays a critical role in this process, as the epiblast undergoes rosette formation and lumen expansion to form the amniotic cavity. Here, we present a high-throughput *in vitro* model for epiblast morphogenesis. We established a microfluidic workflow to encapsulate human pluripotent stem cells (hPSCs) into monodisperse agarose microgels. Strikingly, hPSCs self-organized into polarized epiblast spheroids that could be maintained in self-renewing and differentiating conditions. Encapsulated primed hPSCs required Rho-associated kinase inhibition, in contrast to naive hPSCs. We applied microgel suspension culture to examine the lumen-forming capacity of hPSCs and reveal an increase in lumenogenesis during the naive-to-primed transition. Finally, we demonstrate the feasibility of co-encapsulating cell types across different lineages and species. Our work provides a foundation for stem cell-based embryo models to interrogate the critical components of human epiblast self-organization and morphogenesis.

INTRODUCTION

The ability of individual cells to amalgamate into an epithelium and undergo lumenogenesis is of central importance for the formation of multicellular organisms. A prominent example in human development is amniotic cavity formation, where pluripotent epiblast cells form a polarized rosette and subsequently open a central lumen. This process requires the establishment of apical-basal polarity, formation of tight junctions for epithelialization, and lumen expansion. Human embryo culture to postimplantation stages has demonstrated that epiblast lumenogenesis occurs in the absence of maternal tissues, highlighting the intrinsic capacity of self-organization in early embryonic cells (Deglincerti et al., 2016; Shahbazi et al., 2016).

Self-organizing properties extend to embryo-derived and induced pluripotent stem cells (PSCs) (Shahbazi et al., 2017; Simunovic et al., 2019; Taniguchi et al., 2015; Warmflash et al., 2014). PSCs can be captured in naive and primed states of pluripotency, corresponding to the pre- and postimplantation epiblast, respectively (Boroviak et al., 2014; Boroviak and Nichols, 2017; Nakamura et al., 2016; Nichols and Smith, 2009; Takashima et al., 2014; Ying et al., 2008). The preimplantation epiblast is an unpolarized aggregate of cells (Bedzhov and Zernicka-Goetz, 2014; Enders et al., 1986), which is preserved in the characteristic dome-shape morphology of naive PSC colonies (Takashima et al., 2014; Theunissen et al., 2014; Ying et al., 2008). In contrast, primed human PSCs (hPSCs) grow as flat epithelial colonies, thereby recapitulating the tissue architecture of the postimplantation embryo (Brons et al., 2007; Krtolica et al., 2007; Tesar et al., 2007). The developmental stage of pluripotent cells is a critical parameter for self-organization and lumenogenesis. In the human embryo, the naive epiblast undergoes rosette formation and lumen expansion at the peri-implantation stage, giving rise to the embryonic disk and nascent amnion (Boroviak and Nichols, 2017; Enders et al., 1986; Hertig et al., 1956; Ross and Boroviak, 2020; Rossant and Tam, 2018). While naive hPSCs cultured in self-renewing conditions (including MEK inhibition with PD035901) are capable of transient polarization and rosette formation in three-dimensional (3D) cultures, hPSCs must exit naive pluripotency for successful lumen expansion (Shahbazi et al., 2017). This is in contrast to primed hPSCs, which readily undergo lumenogenesis in self-renewing conditions (fibroblast growth factor [FGF] and transforming growth factor β [TGF-β]/NODAL stimulation) within 48 h (Shahbazi et al., 2017). Primed hPSCs have the potential of giving rise to embryonic disk-like structures and amnion *in vitro* (Shao et al, 2017a, 2017b; Zheng et al., 2019), despite their postimplantation epiblast identity (Nakamura et al., 2016). However, the dynamic changes in lumenogenesis between naive and primed pluripotent states have remained unresolved due to the lack of a scalable and robust 3D-culture system for hPSCs.

This is an open access article under the CC BY-NC-ND license (http://creativecommons.org/licenses/by-nc-nd/4.0/).

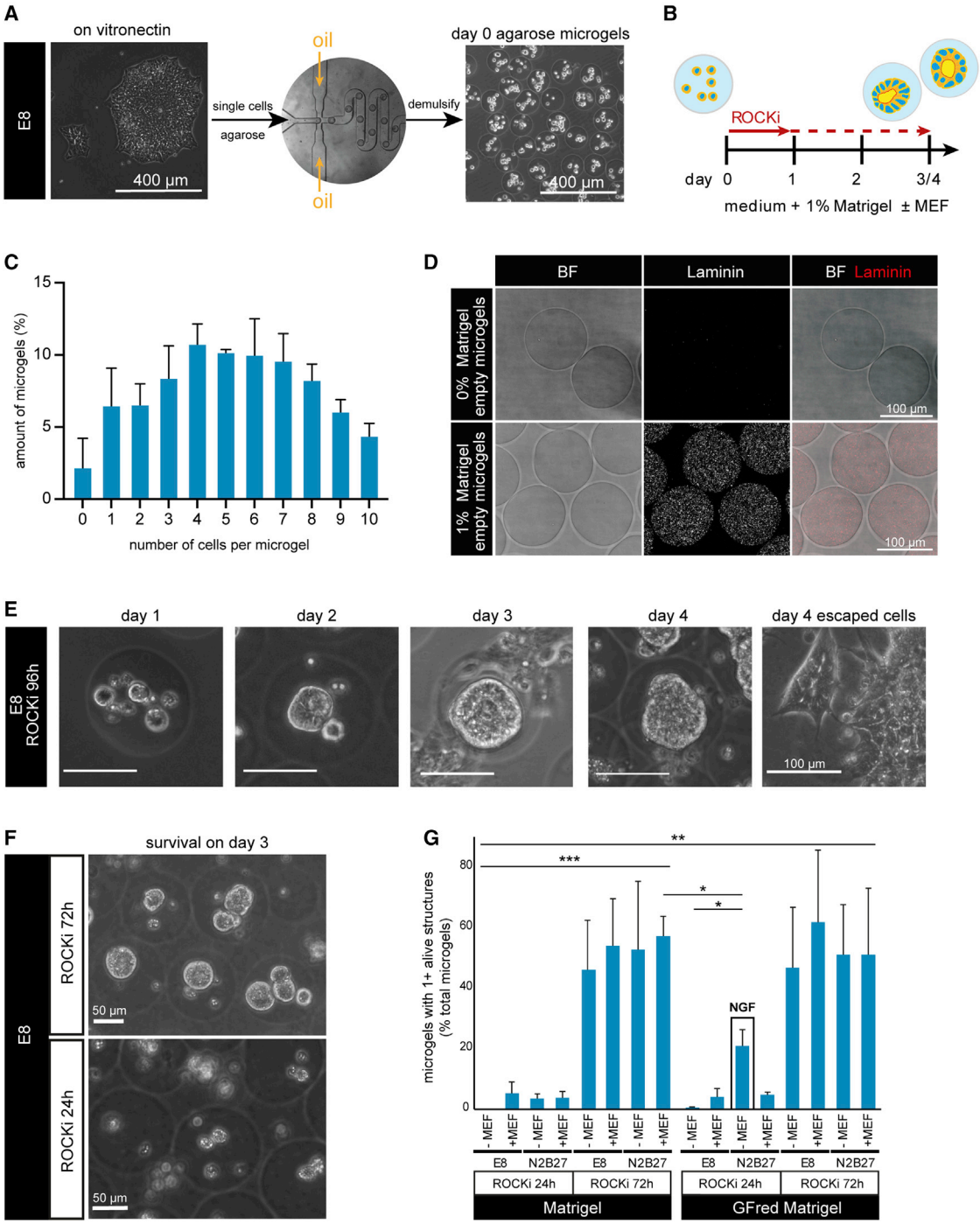

Figure 1. Encapsulation of hPSCs in agarose microgels

(A) Workflow for encapsulating hPSCs into agarose microgels.

(B) Schematic of microgel suspension culture with short-term (solid arrow) versus constant (dashed arrow) ROCK inhibition. MEF, mouse embryonic fibroblasts used as feeder cells.

(C) Quantitative distribution of cell numbers per microgel using 7.5×10^6 cells/mL directly after encapsulation (n = 3). Error bars represent mean + SD.

(D) Brightfield and confocal images of laminin in empty microgels incubated for 2 days with or without Matrigel.

(E) Phase-contrast images of structures from primed hPSCs in microgels developing over time.

(legend continued on next page)

Primed hPSCs establish apical-basal polarity through the formation of an internal perinuclear membrane, the apicosome (Taniguchi et al., 2015, 2017). During mitosis, the apicosome relocates to the cytokinetic plane, where it establishes a fully polarized lumen between the two dividing cells (Taniguchi et al., 2017). This microcyst soon collapses in conventional two-dimensional (2D) monolayer cultures; however, cyst formation and lumenogenesis can be stabilized in 3D cultures of primed hPSCs with Matrigel (Shahbazi et al., 2016, 2017) or Geltrex (Taniguchi et al., 2015). Matrigel is a tumor extract from Engelbreth-Holm-Swarm sarcoma cells that contains basement membrane components and growth factors (Kleinman and Martin, 2005). While Matrigel has enabled a myriad of cell-culture applications, including organoid (Clevers, 2016) and embryo culture (Xiang et al., 2020), its ill-defined and variable composition presents a current limitation for many culture regimes (Aisenbrey and Murphy, 2020). The establishment of synthetic 3D-culture systems will be an important step in delineating the essential extracellular matrix components for lumen formation in the human epiblast.

Survival and proliferation of cells in an epithelium is tightly controlled, which renders primed PSCs vulnerable to programmed cell death after single-cell dissociation (Ohgushi et al., 2010), in contrast to naive cultures (Shahbazi et al., 2017; Takashima et al., 2014; Theunissen et al., 2014). Rho-associated kinase (ROCK) inhibition with Y-27632 restores single-cell survival in primed PSCs (Chen et al., 2010; Watanabe et al., 2007). Moreover, ROCK inhibition promotes lumen formation in hPSCs (Taniguchi et al., 2015; Yu et al., 2008) and Madin-Darby canine kidney (MDCK) cells through inhibition of actin-myosin contractions (Bryant et al., 2014; O'Brien et al., 2001; Yu et al., 2008). Similar to MDCK cells, short-term (<24 h) ROCK inhibition increases the levels of Ezrin in primed hPSCs (Taniguchi et al., 2015). However, little is known about the long-term effects of ROCK inhibition on lumenogenesis in self-renewing and differentiating hPSCs.

Microfluidic devices have been extensively used for the generation of monodisperse hydrogel microdroplets to compartmentalize biological and chemical reactions (Fischlechner et al., 2014; Huebner et al, 2007, 2008; Theberge et al., 2010). Recent applications include the encapsulation of dissociated mouse PSCs in agarose microgels to combine live imaging with precise cell retrieval for endpoint analysis (Kleine-Brüggeney et al., 2019; Mulas et al., 2020). Microgels provide a scalable platform from which to study PSCs in the context of a synthetic 3D matrix and represent an exciting avenue to combine embryonic and extraembryonic lineages for stem cell-based embryo models. Nevertheless, protocols for hPSC encapsulation and subsequent microgel suspension culture have remained elusive.

Here, we set out to investigate the self-organizing properties of naive and primed hPSCs in hydrogel droplets. We established a microfluidic platform to encapsulate small populations of hPSCs in agarose microgels in a high-throughput fashion. This approach allowed us to assess self-organization of naive and primed hPSCs into spherical 3D structures under self-renewing and differentiating conditions. We demonstrate that prolonged ROCK inhibition compromises the formation of spheres with one central lumen in differentiating conditions and reveal an increase in the lumen-forming capacity in primed versus naive hPSCs. Finally, we show the versatility of agarose microgel suspension culture by co-encapsulating hPSCs with mouse extraembryonic endoderm (mXEN) cells. Our work provides a powerful experimental framework with which to interrogate self-organization of embryo-derived cells and their responses to physical and chemical stimuli.

RESULTS

hPSCs form 3D structures in agarose microgels

We encapsulated hPSCs in agarose microgels to investigate epiblast morphogenesis in a chemically defined 3D scaffold (Kleine-Brüggeney et al., 2019; Mulas et al., 2020) (Figure 1A). Primed hPSCs cultured in self-renewing conditions (Essential 8 medium [E8]) (Chen et al., 2011) were dissociated to single-cell suspension and mixed with a low-melting-point agarose solution. Monodisperse water-in-oil emulsion droplets were formed in microfluidic polydimethylsiloxane devices (>200 droplets per second) from two streams of aqueous and oil phases by break-off flow (Video S1 and experimental procedures). After polymerization, the resulting cell-containing microgels were transferred into conventional tissue-culture plates for further culture (Figure 1B). hPSC encapsulation dynamics followed a Poisson distribution (Huebner et al., 2007) (Figure S1A), which enables tight control over the number of cells per microgel over a wide range of concentrations (Figure S1B). We optimized the concentration of hPSCs in

(F) Phase-contrast images of primed hPSCs in microgels with (top) and without (bottom) constant ROCK inhibition at day 3.
(G) Quantification of cell survival of primed hPSCs in microgels with 1% Matrigel (n = 3 hPSC encapsulation experiments) or growth factor reduced Matrigel (n = 2 hPSC encapsulation experiments) on day 3. GFred Matrigel, growth factor reduced Matrigel. Significance was calculated between pooled samples containing Matrigel ROCKi 24 h, Matrigel ROCKi 72 h, GFred Matrigel ROCKi 24 h, or GFred Matrigel ROCKi 72 h using ANOVA followed by Tukey-Kramer analysis. Additional comparisons were conducted between NGF and all other conditions using ANOVA followed by Tukey-Kramer analysis. Error bars represent mean + SD (*p < 0.05, **p < 0.01, ***p < 0.001).

medium/agarose solution to 7.5 × 10^6 cells/mL for efficient cell encapsulation and survival, resulting in 4–6 cells per microgel on average (Figure 1C). Agarose microgels were monodisperse with a uniform diameter of 100 μm, stable to mechanical manipulation, and could be handled by either conventional or mouth pipetting for subsequent experimental procedures.

Agarose is biologically inert and therefore unable to support cell adhesions. Primed hPSCs exhibit apical-basal polarity and integrin-dependent matrix adhesion (Krtolica et al., 2007; Shahbazi et al., 2017), similar to the columnar epithelium of the human embryonic disk (Boroviak and Nichols, 2017). To facilitate 3D-structure formation of encapsulated hPSCs, we supplemented the medium with low concentrations of Matrigel (Figures S1C and S1D). We confirmed efficient perfusion of 1% Matrigel by laminin immunofluorescence in empty agarose microgels (Figure 1D). hPSCs aggregated and formed radial structures after 24 h in self-renewing culture conditions (E8) (Figure 1E). At day 4, the structures began to escape from the agarose microgels due to their size and attached to the bottom of the dish (Figure 1E). We therefore examined hPSC-containing microgels primarily before day 4. To optimize 3D-structure formation as a model for epiblast lumenogenesis, we screened multiple culture regimes and assessed hPSC-derived structures at day 3. Experimental conditions included serum-free self-renewing (E8) and differentiation-permissive conditions (N2B27 medium), short-term (24 h) versus constant (72 h) ROCK inhibition (ROCK inhibitor Y-27632), and the presence or absence of a layer of mitotically inactivated mouse embryonic fibroblasts (MEFs) at the bottom of the dish (Figures 1E, 1G, S1, and S2). Image quantification showed robust 3D-structure formation (>50%) in E8 and N2B27, either with or without MEFs (Figure 1G). However, 3D-structure formation of encapsulated primed hPSCs was consistently higher with constant (72 h) ROCK inhibition, compared with short-term (24 h) ROCK inhibition (Figures 1F, 1G, S1C, S2A, and S2B).

Prolonged ROCK inhibition has been reported to affect the metabolism, pluripotency, and cytoskeleton in hPSCs (Gao et al., 2019; Vernardis et al., 2017). To evaluate any potential side effects in encapsulated hPSCs, we aimed to establish microgel culture conditions permitting 3D-structure formation without constant ROCK inhibition. We found that replacing 1% conventional Matrigel in N2B27 with growth factor reduced Matrigel could partially rescue cell survival (>20%) in microgel cultures with brief ROCK inhibition (NGF: N2B27, growth factor reduced Matrigel, and feeder-free microgel suspension culture; Figure 1G). However, growth factor reduced Matrigel did not improve survival in E8 (Figure 1G). We conclude that agarose microgels accommodate primed hPSCs to form 3D structures in self-renewing and differentiating conditions, providing a high-throughput platform for morphological analysis.

Lumen formation is a hallmark of hPSC microgel suspension culture

hPSC-derived 3D structures appeared radial and homogeneous in agarose microgels (Figure 1E). To determine the cellular architecture of the encapsulated 3D structures, we performed whole-mount confocal immunofluorescence staining with the pluripotency marker OCT4, the apical tight junction protein ZO-1 (Bryant and Mostov, 2008), and β-catenin to highlight adherens junctions (Figures 2A and S3). The majority of encapsulated hPSCs formed polarized spheroids with a ZO1-positive lumen (Figure 2A). In self-renewing culture conditions, the pluripotency marker OCT4 was robustly expressed but downregulated in differentiation-permissive N2B27 medium (Figures 2A and 2B). Fluorescence quantification showed that OCT4 levels were further reduced on day 4. Matrigel versus growth factor reduced Matrigel did not change this pattern (Figures 2A, 2B, and S3). Collectively, these observations suggest that agarose-encapsulated primed hPSCs self-organize into spheroids and undergo lumen expansion in self-renewing and differentiating conditions.

Constant ROCK inhibition compromises single lumen formation in differentiating conditions

Image analysis based on the localization of the apical polarity marker ZO-1 (Figure 3A) confirmed spheroid formation in the majority of agarose microgels cultured in self-renewing (E8) and differentiating (N2B27) conditions (>68%, n = 965 across nine experimental conditions, Figure 3B). The abundant formation of ZO-1-positive lumen demonstrates that long-term (96 h) ROCK inhibition did not interfere with lumenogenesis (Figure 3B). However, prolonged ROCK inhibition has been reported to induce cytoskeletal aberrations (Chen et al., 2010; Gao et al., 2019), so we performed quantitative image analysis to examine lumen morphology in greater detail. We categorized spheroids into (1) single lumen and (2) multiple lumina structures (Figure 3C). All self-renewing conditions (E8 ± MEFs, Matrigel, or GF Red Matrigel) required constant ROCK inhibition and gave rise to predominantly single polarized lumina, but also some structures with multiple lumina (Figure 3D). In differentiating conditions (N2B27 ± MEFs, Matrigel, or GF Red Matrigel) with constant ROCK inhibition, 3D structures showed a mixture of single and multiple lumina, particularly in the presence of MEFs. However, microgel cultures without constant ROCK inhibition exclusively formed structures with a single polarized lumen in NGF conditions (Figure 3D; see also Figure 1E). A subset of spheroids gave rise to hollow structures in the absence of apical polarity marker ZO-1 (Figure 3E). The formation of these

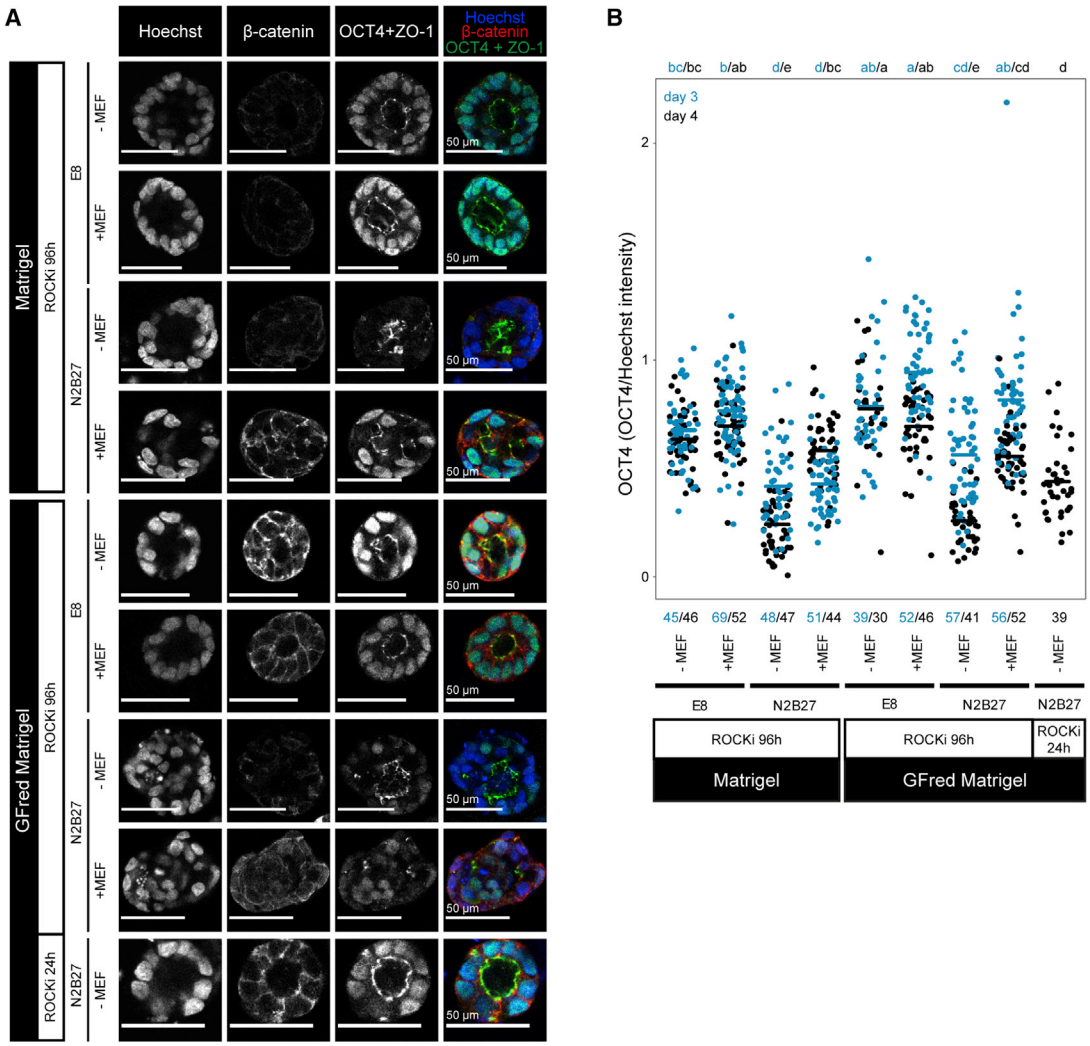

Figure 2. Self-organization of encapsulated hPSCs into spheroids

(A) Immunofluorescence images of primed hPSC-derived cultured in agarose microgels with Matrigel or growth factor reduced Matrigel on day 4.

(B) Quantification of OCT4 fluorescence intensity after 3 and 4 days of microgel suspension culture. Figures below plot indicate the numbers of structures measured for each condition. Significance level between days 3 and 4 was calculated using Welch's t test (*$p < 0.05$, **$p < 0.01$, ***$p < 0.001$). Statistics were calculated using ANOVA followed by Tukey-Kramer analysis (samples with the same letter assigned show no significant difference of $p \leq 0.01$).

disorganized cavities was highest in differentiating conditions with MEFs and absent in NGF spheroids (Figure 3F).

Intrigued by the uniform morphology of hPSCs in NGF, we decided to further characterize NGF spheroids at day 4 (Figure 4A). NGF spheroids expressed the pluripotency factors OCT4 and SOX2 (Figure 4B), suggesting epiblast, rather than amnion, identity (Sasaki et al., 2016). This was consistent with the columnar epithelial architecture of NGF spheroids. Cell membranes at the inside of the central lumen were positive for the apical polarity proteins PAR6 and Ezrin (Figure 4B). Quantification of nuclear orientation showed substantial differences between NGF spheroids and structures grown in feeder-free culture regimes with constant ROCK inhibition (Figure 4C). NGF structures formed single-layered columnar epithelia with more consistent nuclear orientation toward the center of the lumen. This demonstrates that constant ROCK inhibition affects the formation of a central polarized lumen of epiblast spheroids in agarose microgels under differentiating conditions.

Resetting to naive pluripotency enhances cell survival in agarose microgels

Naive hPSCs correspond to the preimplantation epiblast prior to epithelial formation. We hypothesized that naive

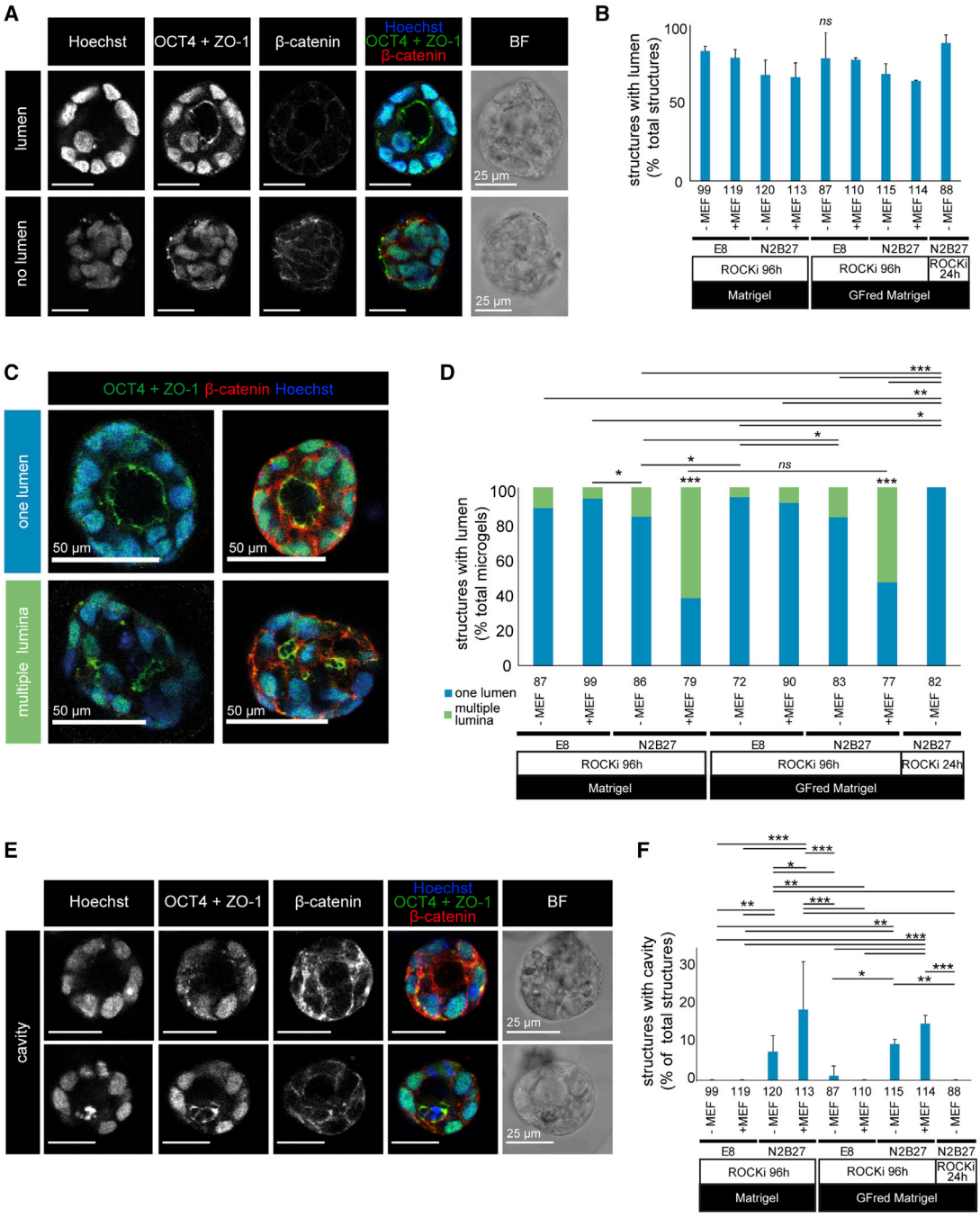

Figure 3. Prolonged ROCK inhibition affects lumen formation

(A) Immunofluorescence images of structures with (top) or without (bottom) lumen formed by encapsulated hPSCs in E8 with MEF and constant ROCK inhibition.

(B) Quantification of lumen formation by structures from primed hPSCs on day 4 (n = 2 hPSC encapsulation experiments).

(C and D) Representative images (C) and quantification (D) of structures with single or multiple lumen formed by primed hPSCs in microgels at day 4 (n = 2 hPSC encapsulation experiments).

(legend continued on next page)

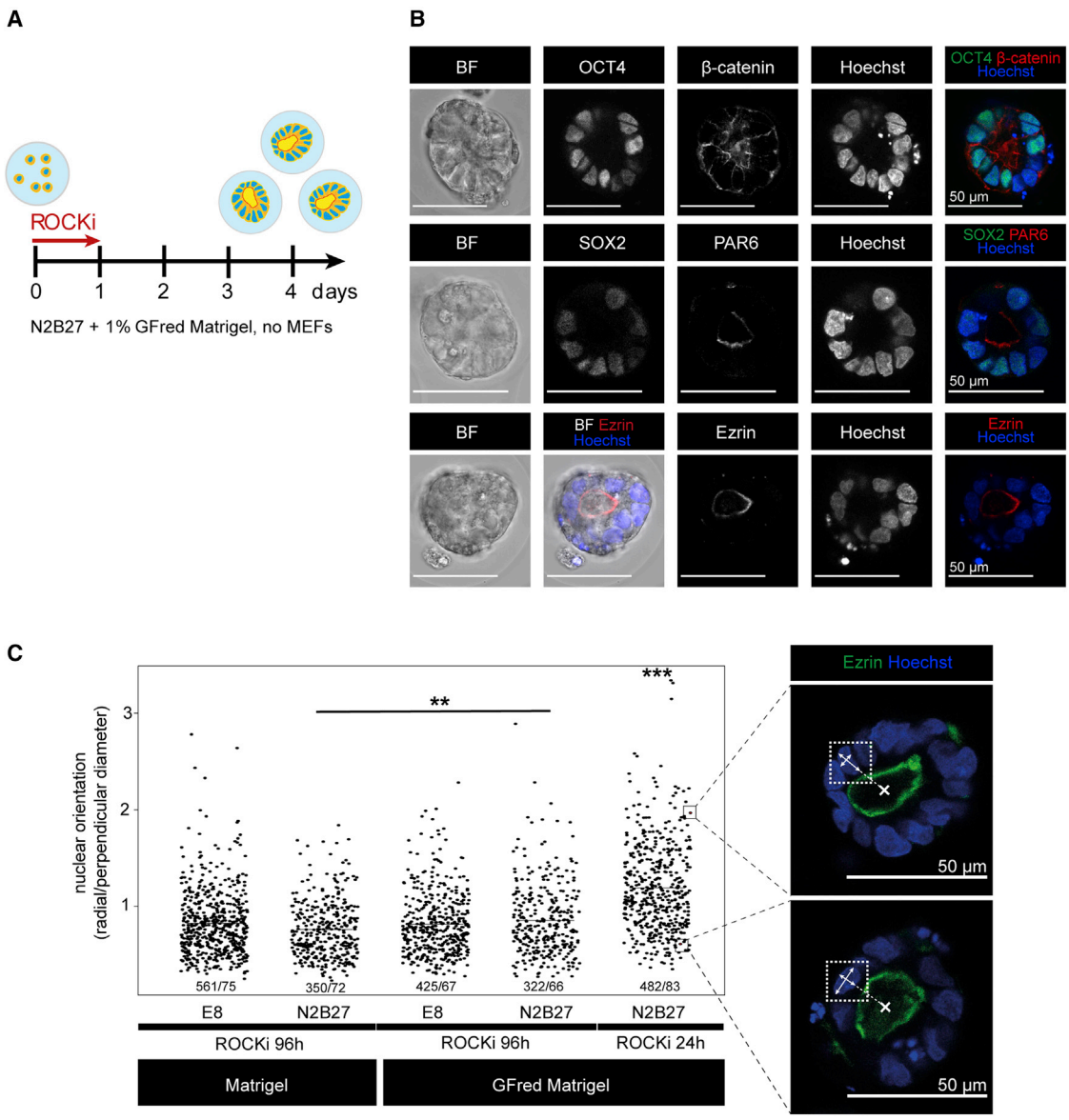

Figure 4. hPSCs form highly organized spheroids in agarose microgels

(A) Schematic of NGF (N2B27, growth factor reduced Matrigel, feeder-free) microgel suspension culture.

(B) Immunofluorescence images of encapsulated primed hPSCs cultured for 4 days in NGF conditions and 24-h ROCK inhibition.

(C) Quantification of nuclear orientation in structures from primed hPSCs (n = 2 hPSC encapsulation experiments). GFred Matrigel, growth factor reduced Matrigel. Statistics were calculated using ANOVA followed by Tukey-Kramer analysis (**p < 0.01, ***p < 0.001). Numbers below the scatterplot represent the number of nuclei/structures quantified in each condition.

hPSCs would readily survive in agarose microgels without the need for constant ROCK inhibition and may provide a developmentally earlier model for lumenogenesis. We generated naive hPSCs by chemical resetting using PXGL (PD0325901, XAV939, Gö6983, human leukemia inhibitory factor [LIF]) in N2B27 on MEFs (Bredenkamp et al.,

(E and F) Representative images (E) and quantification (F) of structures with cavities (ZO-1 negative) formed by primed hPSCs in microgels at day 4 (n = 2 hPSC encapsulation experiments). Numbers below the plots represent numbers of structures quantified in each condition. GFred Matrigel, growth factor reduced Matrigel.

Statistical analysis used pairwise Fisher's tests (*p < 0.05, **p < 0.01, ***p < 0.001; ns, not significant; samples with the same letter assigned show no significant difference of $p \leq 0.05$).

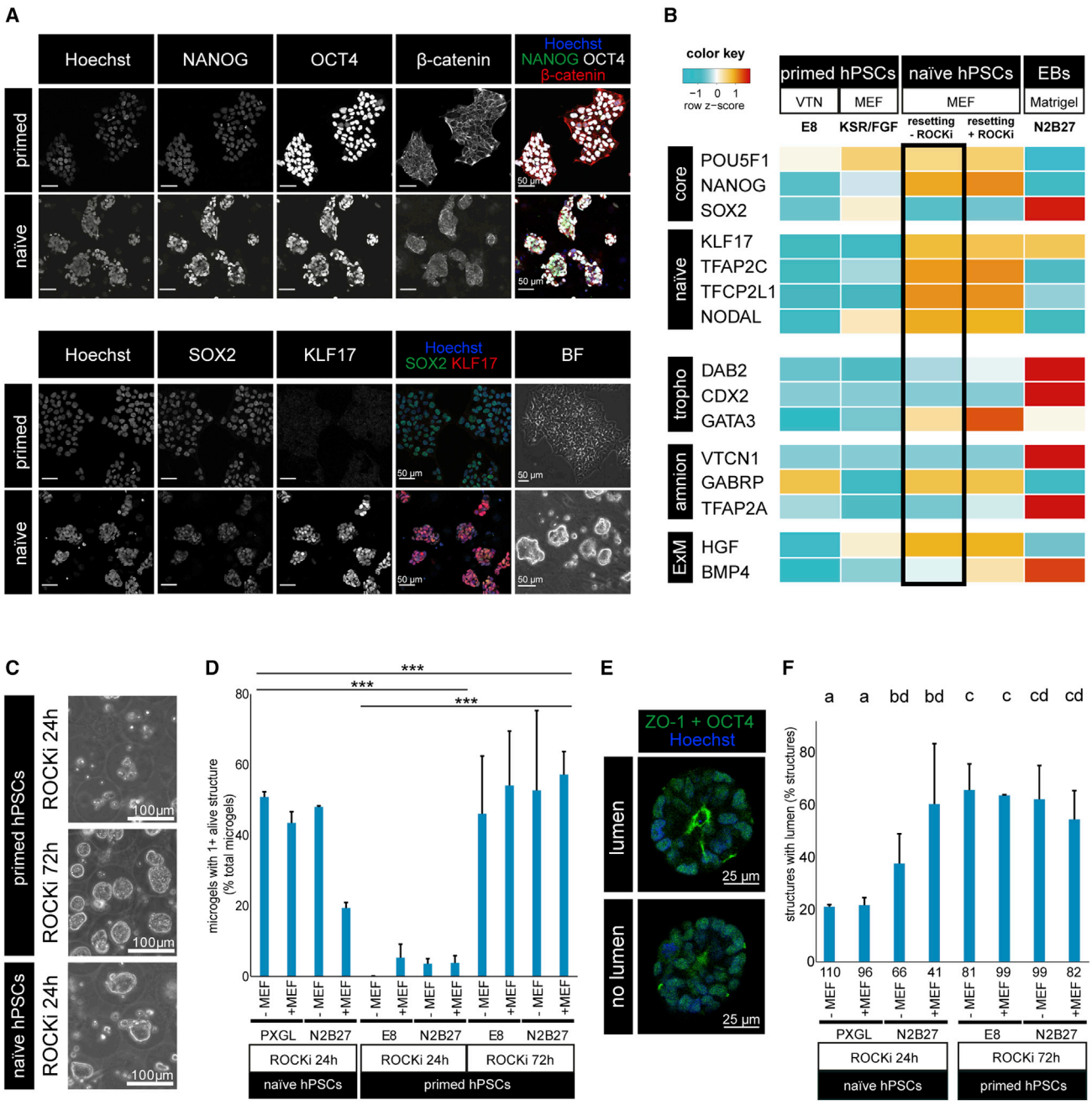

Figure 5. Naive hPSCs robustly survive in agarose microgels and undergo lumenogenesis in differentiating conditions

(A) Immunofluorescence images of naive and primed hPSCs for the lineage markers indicated.

(B) Relative mRNA levels as determined by quantitative RT-PCR of primed and naive hPSCs treated with or without ROCK inhibitor (ROCKi) during the first 10 days of resetting. VTN, vitronectin; MEF, mouse embryonic fibroblasts (n = 2 hPSC encapsulation experiments). Naive cells were reset with and without ROCKi.

(C and D) Phase-contrast images (C) and quantification (D) of survival of naive (n = 2 hPSC encapsulation experiments) and primed (n = 3 hPSC encapsulation experiments) hPSCs in microgels in different conditions supplemented with regular Matrigel on day 3. Significance was calculated between pooled naive hPSCs 24-h ROCKi, primed hPSCs 24-h ROCKi, and primed hPSCs 72-h ROCKi samples using ANOVA followed by Tukey-Kramer analysis (**$p < 0.01$, ***$p < 0.001$).

(legend continued on next page)

2019; Guo et al., 2017). Naive hPSCs exhibited a dome-shaped morphology one to two passages after resetting. Immunofluorescence in naive and primed hPSCs showed robust expression of the core pluripotency factors OCT4, NANOG, and SOX2 (Nichols and Smith, 2009), but only naive hPSCs expressed the naive marker KLF17 (Blakeley et al., 2015; Boroviak et al., 2018; Stirparo et al., 2018) (Figure 5A). Quantitative RT-PCR confirmed upregulation of naive pluripotency markers *TFCP2L1*, *TFAP2C*, and *NODAL* (Boroviak et al., 2018; Nakamura et al., 2016; Pastor et al., 2018) in chemically reset hPSCs generated with and without ROCK inhibition (Figure 5B). Extraembryonic lineage specifiers were lowly expressed in comparison with random embryoid body differentiation, although we detected an increase in *GATA3* levels, consistent with the recently reported trophoblast potential of naive hPSCs (Dong et al., 2020; Guo et al., 2020) (Figure 5B).

To examine lumenogenesis in the context of naive pluripotency, we encapsulated naive hPSCs into agarose microgels and cultured them for 3 days in self-renewing (PXGL medium) and differentiating (N2B27) conditions in the presence and absence of MEFs (Figures 5C, 5D, S4A, and S5B). Naive hPSCs in self-renewing conditions exhibited survival rates similar to those of primed cells with constant ROCK inhibition (Figures 5C and 5D). We assessed lumen formation by confocal immunofluorescence of ZO-1 and OCT4 and observed either small or no lumina in the 3D structures (Figure 5E). Encapsulated naive hPSCs cultured in self-renewing conditions exhibited the least number of structures with lumen, followed by naive hPSCs in differentiating conditions. Interestingly, primed hPSCs exhibited the highest percentage of lumen formation (Figures 5F and S4B). These findings are consistent with mouse and human PSCs embedded in Matrigel, where lumen expansion was only observed after exit from naive pluripotency (Shahbazi et al., 2017). We conclude that microgel spheroids from naive hPSCs do not require constant ROCK inhibition and are capable of lumenogenesis in differentiating conditions.

Naive and primed epiblast spheroids differ in lineage potential

We investigated the developmental capacity of epiblast spheroids from naive and primed hPSCs by lineage marker analysis in self-renewing and differentiating conditions. Spheroids from naive hPSCs exhibited OCT4 expression across conditions (Figures 6A and S4C–S4E), consistent with epiblast identity. Immunofluorescence intensity quantification revealed that OCT4 levels decreased in the presence of MEFs (Figure S4C), and the naive pluripotency factor KLF17 showed a downward trend in N2B27 with MEFs (Figures 6A and S4E). Epiblast spheroids in differentiating conditions with feeders, but not self-renewing conditions, upregulated the early mesoderm marker TBXT (Figures 6A and S4D), which is expressed in the primate amnion and embryonic disk during gastrulation (Nakamura et al., 2016; Sasaki et al., 2016). We performed time-course analysis for naive hPSCs in agarose microgels at day 2 and day 3 after encapsulation and examined SOX2, ZO-1, TBXT, and the naive pluripotency and amnion marker TFAP2C (AP2-γ) (Figures S5A–S5C). We consistently found that naive hPSCs in self-renewing conditions (PXGL) form polarized rosettes but do not undergo lumen expansion. Naive hPSCs expressed lower levels of SOX2 but higher levels of TFAP2C compared with primed hPSCs. At day 2, there was a trend toward higher TFAP2C levels in self-renewing versus differentiating conditions, which led to a significant increase at day 3. Together with the morphological feature of an unopened lumen and KLF17 expression, this suggests that naive hPSC-derived structures in PXGL maintain their naive pluripotent state rather than undergoing amnion differentiation.

Naive hPSC-derived 3D structures exclusively expressed TBXT in differentiating conditions in the presence of feeders (N2B27/24-h ROCK inhibition/1% growth factor reduced Matrigel) (Figures 6A and S5A–S5C). This led us to examine microgel cultures from primed hPSCs cultured in the same conditions. Epiblast spheroids from primed hPSCs exhibited robust SOX2 expression, low levels of TFAP2C, and complete absence of TBXT (Figure 6B). To assess whether primed hPSCs were capable of mesodermal lineage entry in agarose microgels, we pulsed suspension cultures for the first 24 h with the WNT agonist CHIR99021. WNT signaling is critical for mouse and human mesoderm induction and primitive streak formation in the posterior epiblast (Arnold and Robertson, 2009; Martyn et al., 2019; Moris et al., 2020; Nakamura et al., 2016). Confocal imaging and fluorescence intensity quantification showed that CHIR99021 treatment led to a dramatic upregulation of TBXT in encapsulated primed hPSCs (Figures S6A and S6D). Extending CHIR99021 treatment to 72 h further increased TBXT expression (Figures S6A and S6C). TBXT-positive 3D structures from CHIR99021-induced primed hPSCs did not undergo lumenogenesis and grew as cell aggregates, consistent with mesodermal lineage entry. In contrast, CHIR99021-treated naive

(E) Immunofluorescence images of spheroids from naive hPSCs in PXGL without MEFs on day 3.

(F) Quantification of lumen formation in spheroids from naive hPSCs from two encapsulation experiments (n = 2 hPSC encapsulation experiments). Figures below each bar indicate the total number of spheroids analyzed. Statistics were calculated using pairwise Fisher's tests (samples with the same letter assigned show no significant difference of $p \leq 0.05$). Error bars represent mean + SD.

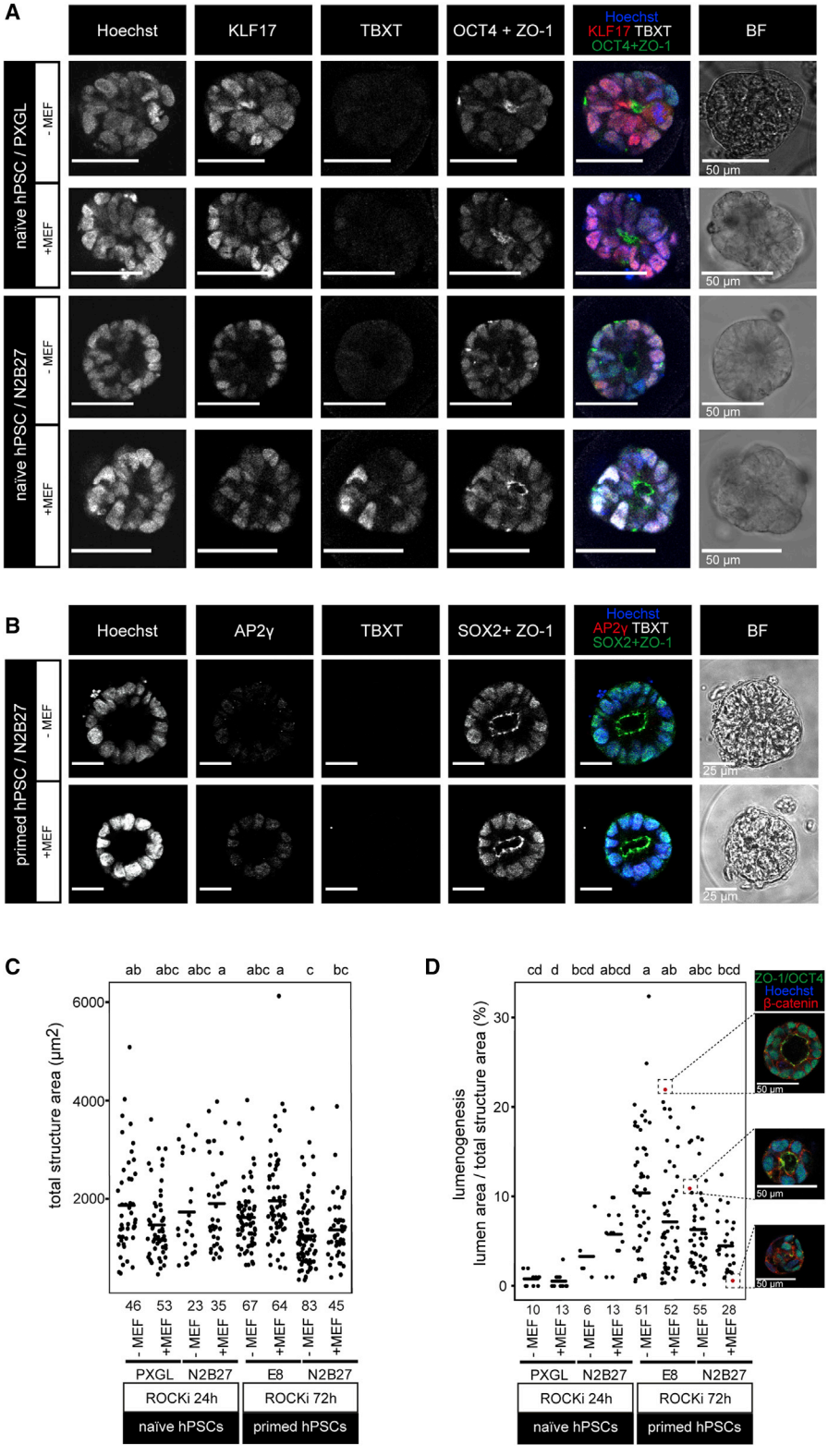

(legend on next page)

hPSCs did not survive (Figures S6A–S6D). Collectively, the observed differences in lineage marker acquisition demonstrate profound divergence in the developmental potential of naive and primed hPSC-derived microgel cultures.

Lumen expansion increases in the naive-to-primed transition

To determine the lumen-forming capacity of naive and primed hPSCs, we compared hPSCs from both developmental states (Figures 6C and 6D). Microgel 3D structures were cultured in self-renewing (PXGL for naive, E8 for primed) and differentiating (N2B27) conditions in the presence and absence of MEFs. We measured the total structure area of confocal mid-sections of the relevant 3D structures and found no differences between experimental conditions (Figure 6C). This suggested that the size of microgel 3D structures was independent of the pluripotency state.

We then examined the ratio of lumen area to total structure area for those 3D structures that had undergone lumen expansion. Encapsulated naive hPSCs in self-renewing conditions produced hardly any lumen (Figure 6C, <0.8% of the total area). Switching from naive to differentiating N2B27 conditions allowed the rosettes to open and led to increased lumen formation (~4%), particularly in the presence of MEFs (~6%, Figure 6C). Strikingly, the capacity for lumenogenesis was largest in 3D structures obtained from primed hPSCs. Self-renewing and differentiating conditions in primed hPSCs exhibited high lumen-to-structure-area ratios (~5%–8%) in general, but the largest lumina were generated from primed hPSCs in E8 without MEFs (~11%) (Figure 6C). This demonstrates a substantial increase in the lumen-forming capacity during the naive-to-primed transition in hPSCs.

Co-encapsulations across lineage and species boundaries

Embryogenesis is orchestrated through dynamic signals at the interface of embryonic and extraembryonic tissues. In the peri-implantation embryo, the epiblast compartment is partially surrounded by extraembryonic endoderm. Droplet microfluidics presents an exciting opportunity to develop scalable co-cultures of cell types from different lineages or species. To demonstrate the flexibility of our microfluidic system, we co-encapsulated primed hPSCs with GFP-labeled mXEN cells (Figure 7A). We screened self-renewing and differentiating culture conditions, with and without 20% fetal bovine serum and 24 h versus constant ROCK inhibition (Figures 1B, 7A, 7B, and S7). mXEN cells survived in all experimental conditions (Figure 7B). Co-encapsulated hPSCs required constant ROCK inhibition (Figure 7B), in accordance with our previous results (Figures 1F and 1G). We robustly obtained chimeric structures in serum-free E8 and N2B27 with constant ROCK inhibition (Figures 7A and 7B). This provides a proof of principle for the efficient generation of compartmentalized embryonic and extraembryonic co-cultures in agarose microgels across species boundaries.

DISCUSSION

This work establishes a high-throughput microfluidic platform to encapsulate hPSCs for agarose microgel suspension culture (Figure 7C). Our approach has provided insights into the lumen-forming potential of naive and primed pluripotent states and provides a versatile experimental system to identify the critical components of human epiblast self-organization. Nevertheless, semi-automated image acquisition and quantification still presents a hurdle to realizing the full high-throughput potential of microgel suspension cultures. Possible solutions could include microfluidic platforms for live-cell imaging combined with microgel retrieval for molecular endpoint analysis (Mulas et al., 2020) or machine-learning algorithms for automated image quantification (Tokuoka et al., 2020).

Lumenogenesis of mouse PSCs or hPSCs has previously relied on the presence of polymerized Matrigel (Bedzhov and Zernicka-Goetz, 2014; Deglincerti et al., 2016; Shao et al., 2017b; Taniguchi et al, 2015, 2017; Zheng et al., 2019). Matrigel is limited in its applicability to study epiblast morphogenesis, due to its complex, ill-defined, and variable composition (Aisenbrey and Murphy, 2020). We obtained better cell survival and 3D-structure formation with growth factor reduced Matrigel. This is surprising and may be caused by batch-to-batch variation or incompatible signaling crosstalk with an unidentified growth factor. In contrast, agarose microgels consist of biologically inert hydrogels. The agarose pore diameter of 200 nm ensures efficient perfusion of culture medium and extracellular matrix components, which we have leveraged to

Figure 6. Lumen formation increases in the naive-to-primed transition

(A) Immunofluorescence images of encapsulated naive hPSCs at day 3.

(B) Immunofluorescence images of encapsulated primed hPSCs at day 3.

(C and D) Quantification of total spheroid area (C) and relative lumen size (D) of spheroids in naive and primed hPSCs from two encapsulations (shown from n = 1 hPSC encapsulation experiments). Statistics were calculated using an ANOVA test followed by Tukey-Kramer analysis (samples with the same letter assigned show no significant difference of $p \leq 0.05$). Numbers below the plots represent numbers of 3D structures quantified in each condition.

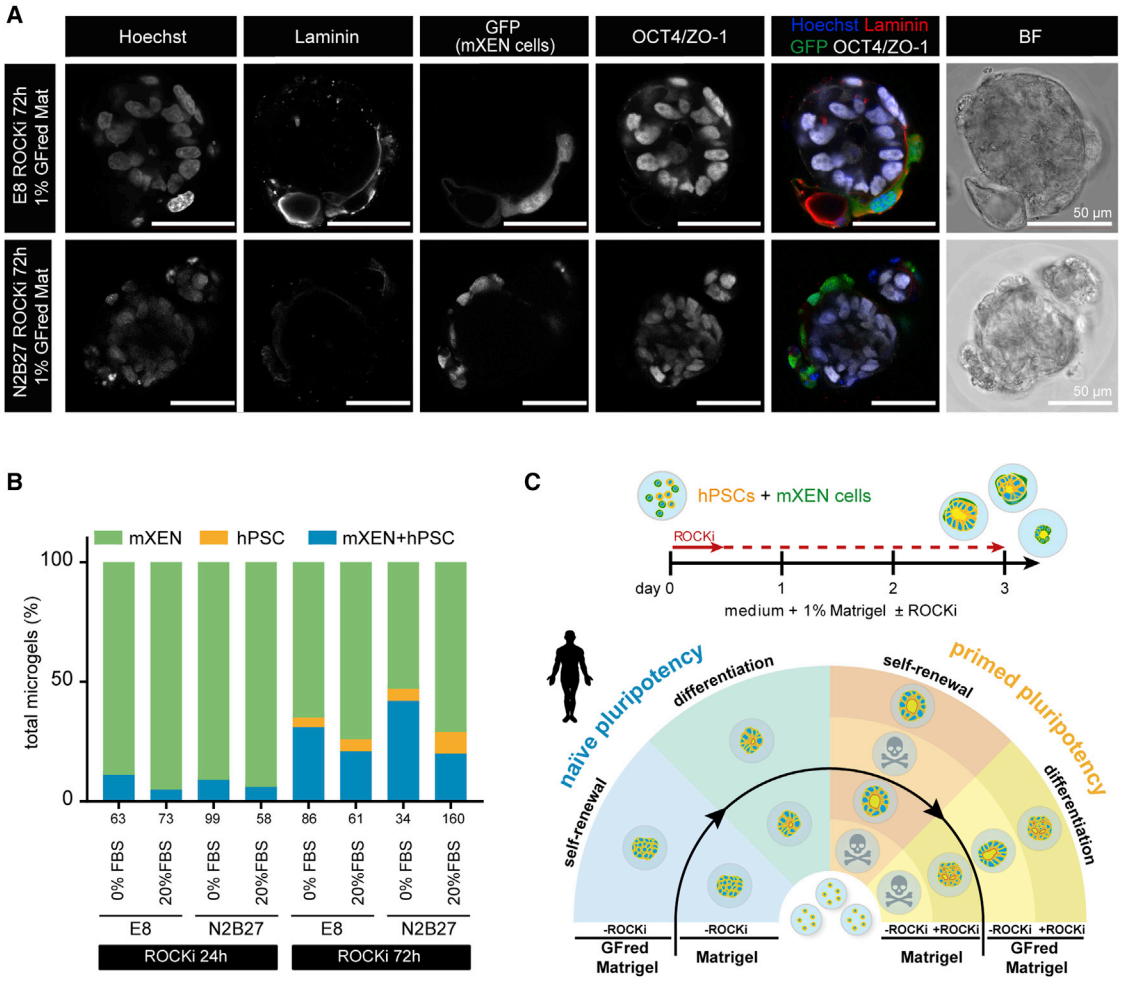

Figure 7. Agarose microgels as a platform for epiblast morphogenesis

(A) Immunofluorescence images of co-encapsulated primed hPSCs and GFP-labeled mXEN after 3 days of co-culture.

(B) Quantification of mXEN, hPSC, and hPSCs + mXEN co-cultures at day 3. Numbers below the plots indicate numbers of structures quantified in each condition (n = 1 hPSC encapsulation experiment).

(C) Schematic summary of co-encapsulations and 3D structures obtained from hPSCs cultured in microgels in the experimental conditions examined in this study. Maintenance and differentiation conditions correspond to PXGL (naive)/E8 (primed) and N2B27, respectively. Red inner linings demarcate the apical lumen.

substantially reduce the amount of Matrigel required for robust epiblast 3D culture. Future avenues toward a biomimetic 3D platform to delineate developmental processes may include the addition of defined extracellular matrix components into the culture medium or the generation of agarose conjugates with extracellular matrix proteins.

Supplementing Matrigel in the medium also allowed us to start to deconvolute physical and biochemical effects, e.g., matrix adhesion-dependent and -independent effects. Soluble Matrigel components inside the microgel are unable to bind to chemically inert agarose. hPSCs bind to Matrigel but not agarose. Thus, the formation of epiblast spheroids did not depend on tension through adhesion to the gel matrix, i.e., "pulling" on the agarose. This conclusion could have not been drawn from 3D cultures embedded in pure Matrigel, where all extracellular matrix components are linked together.

Our current microgel suspension culture heavily relies on ROCK inhibition for robust cell survival of primed hPSCs. Prolonged ROCK inhibition has been reported to reduce key metabolic functions, including glycolysis and the citric acid cycle, as well as the metabolic regulator *mTORC1* (Vernardis et al., 2017) and human blastoid formation (Yu et al., 2021). Moreover, ROCK inhibition profoundly impacts the cytoskeletal architecture of the cell and may substantially reduce the stiffness of the cell

cortex (Srinivasan et al., 2017). The establishment of an optimized and fully defined agarose microgel culture system may eliminate the need for prolonged ROCK inhibition and will provide a scalable platform for genome-wide interrogation of the regulatory networks controlling epiblast lumenogenesis.

Naive and primed hPSCs were able to undergo lumen formation and exit pluripotency dependent on the culture environment (Figure 7C). Apical-basal polarity and rosette formation were frequently observed in naive self-renewing conditions, but in the absence of lumen expansion. This is consistent with a previous report using a Matrigel-based 3D-culture system (Shahbazi et al., 2016, 2017) and highlights the functional importance of naive pluripotency in preventing lumenogenesis. Primed hPSCs showed the greatest capacity for lumenogenesis. This inherent capacity of primed hPSCs for lumen formation is consistent with the massive expansion of the amniotic cavity in the first week of human postimplantation development (Boroviak and Nichols, 2017; Luckett, 1978; Rock and Hertig, 1948). Epiblast spheroids expressed the pluripotency regulators OCT4 and SOX2, pointing toward embryonic disk identity (Nakamura et al., 2016; Tyser et al., 2020). Notably, both self-renewing and differentiating conditions were permissive for spheroid formation. This demonstrates that FGF and TGF-β/NODAL stimulation are compatible with lumenogenesis. The physiological relevance of these pathways is underlined by the pronounced expression of *NODAL* and *FGF4* in the embryonic disk of human (Tyser et al., 2020) and non-human primate (Nakamura et al., 2016) embryos. Future studies will be required to elucidate the downstream targets of FGF and TGF-β/NODAL in the context of lumen expansion.

Encapsulating hPSCs in agarose microgels presents new opportunities for the emerging field of stem cell-based embryology. Currently, the majority of *in vitro* models for human embryogenesis are based on embedding cells in polymerized Matrigel (Moris et al., 2020; Shao et al, 2017a, 2017b; Simunovic et al., 2019). The modularity of agarose microgels, which can be handled and analyzed individually, is a key advantage for the controlled assembly of integrated stem cell-based embryo models. We demonstrated the flexibility of our agarose microgel suspension culture regime by co-encapsulation of hPSCs with mXEN cells. In the future, encapsulated epiblast spheroids could be co-cultured with various extraembryonic stem cell lines, either within the same microgel to investigate direct cell-to-cell interactions or in separate microgels to examine the paracrine signals controlling lineage decisions. Agarose microgels could be readily immobilized in microdevices (Kleine-Brüggeney et al., 2019) or by embedding into defined matrices and exposed to signaling gradients to model gastrulation and amnion formation. This approach will be particularly powerful when combined with live-cell imaging and single-cell transcriptome analysis.

Collectively, we have established the requisite technical protocols for the high-throughput generation of the human peri-implantation epiblast compartment in monodisperse microgels. This experimental platform will provide a versatile system for the functional interrogation of epiblast morphogenesis, lineage acquisition, and self-organization.

EXPERIMENTAL PROCEDURES

Pluripotent stem cell culture

All hPSC experiments were approved by the UK Stem Cell Bank Steering Committee and comply with the regulations of the UK Code of Practice for the Use of Human Stem Cell Lines. Conventional SHEF6 (International Stem Cell et al., 2007), RUES2, and RUES-GLR (obtained with kind permission from the A.H. Brivanlou laboratory, Rockefeller University) were cultured on vitronectin-coated dishes (10 μg/mL; Thermo Fisher Scientific) in E8 medium (Thermo Fisher Scientific) under hypoxic conditions (37°C, 5% CO_2, 5% O_2). Cells were routinely passaged in clumps using 50 mM EDTA.

Naive cells were maintained in PXGL (1 μM PD0325901, 2 μM XAV939, 2 μM Gö6983, and 10 ng/mL human LIF in N2B27) on mitomycin C (Sigma) inactivated MEFs (Cambridge Stem Cell Institute) and passaged with Accutase (Thermo Fisher Scientific). Y-27632 (10 μM) was supplemented during the first 24 h after passage. PD0325901, basic FGF, XAV939, Gö6983, and human LIF were obtained from the Cambridge Stem Cell Institute.

Cell encapsulation

Cells were encapsulated as previously described (Kleine-Brüggeney et al., 2019). In brief, flow focusing in a microfluidic device was used to achieve agarose droplet formation (Anna et al., 2003). Microfluidic devices were made from polydimethylsiloxane and had two inlets for an aqueous phase (agarose + cells) and a continuous oil phase, as well as one outlet for the emulsified droplets. Before encapsulations, cells were single-cell dissociated with Accutase or 0.5 mM EDTA. Cells were resuspended and diluted to 1.5×10^6 cells/100 μL. The cell suspension was mixed 1:1 with a low-melting-point agarose solution at 37°C (3% in PBS; SeaPrep ultra-low-melting-point agarose by Lonza). HFE-7500 (Fluorochem) supplemented with surfactant (0.3%; Pico-Surf by Sphere Fluidics) was used as the continuous oil phase. Syringes (SGE Analytical Science) controlled by automated pumps (CETONI, neMYSIS) were used to inject the agarose-cell suspension separately from the oil-surfactant solution into the microfluidic chips for emulsification. Agarose droplets left the microfluidic chip through the outlet and were collected on ice for polymerization. Microgels were then demulsified through liquid-liquid extraction with culture medium and perfluoro-octanol (AlfaAesar). For some experiments, microgels were pooled from three rounds of encapsulations and distributed to the different culture conditions (~5 conditions per encapsulation): E8, N2B27, or PXGL supplemented with 2.5% chemically defined lipids (Thermo Fisher Scientific), 1% penicillin-streptomycin (Thermo Fisher Scientific), 1% Matrigel

(Corning), or growth factor reduced Matrigel (Corning), and 10 μM Y-27632 as indicated with or without MEFs at the bottom of the culture plate. Microgel suspension cultures were cultured at 37°C under hypoxic conditions (5% CO_2). Please refer to supplemental information for co-encapsulation experiments and further experimental procedures.

SUPPLEMENTAL INFORMATION

Supplemental information can be found online at https://doi.org/10.1016/j.stemcr.2021.04.009.

AUTHOR CONTRIBUTIONS

M.S., D.S., and T.N.K. carried out the majority of experiments, analyzed data, prepared figures, and helped with manuscript preparation. E.S., C.M., and A.L.E. carried out experiments, T.E.B. and F.H. conceived the project and wrote the manuscript.

ACKNOWLEDGMENTS

We are grateful to the Magdalena Zernicka-Goetz lab for GFP-labeled mXEN cells and would like to thank the members of the Hollfelder and Boroviak lab for their enthusiasm and critical discussion of the manuscript. This research is generously supported by the Wellcome Trust (WT RG89228 and WT108438/C/15/Z), the Centre for Trophoblast Research, and the European Research Council (695669). T.E.B. is a WT-Royal Society Sir Henry Dale Fellow. AstraZeneca sponsored a PhD studentship for T.N.K.

Received: September 30, 2020
Revised: April 14, 2021
Accepted: April 14, 2021
Published: May 11, 2021

REFERENCES

Aisenbrey, E.A., and Murphy, W.L. (2020). Synthetic alternatives to Matrigel. Nat. Rev. Mater. *5*, 539–551.

Anna, S.L., Bontoux, N., and Stone, H.A. (2003). Formation of dispersions using "flow focusing" in microchannels. Appl. Phys. Lett. *82*, 364.

Arnold, S.J., and Robertson, E.J. (2009). Making a commitment: cell lineage allocation and axis patterning in the early mouse embryo. Nat. Rev. Mol. Cell Biol. *10*, 91–103.

Bedzhov, I., and Zernicka-Goetz, M. (2014). Self-organizing properties of mouse pluripotent cells initiate morphogenesis upon implantation. Cell *156*, 1032–1044.

Blakeley, P., Fogarty, N.M., Del Valle, I., Wamaitha, S.E., Hu, T.X., Elder, K., Snell, P., Christie, L., Robson, P., and Niakan, K.K. (2015). Defining the three cell lineages of the human blastocyst by single-cell RNA-seq. Development *142*, 3151–3165.

Boroviak, T., and Nichols, J. (2017). Primate embryogenesis predicts the hallmarks of human naïve pluripotency. Development *144*, 175–186.

Boroviak, T., Loos, R., Bertone, P., Smith, A., and Nichols, J. (2014). The ability of inner-cell-mass cells to self-renew as embryonic stem cells is acquired following epiblast specification. Nat. Cell Biol. *16*, 516–528.

Boroviak, T., Stirparo, G.G., Dietmann, S., Hernando-Herraez, I., Mohammed, H., Reik, W., Smith, A., Sasaki, E., Nichols, J., and Bertone, P. (2018). Single cell transcriptome analysis of human, marmoset and mouse embryos reveals common and divergent features of preimplantation development. Development *145*, dev167833.

Bredenkamp, N., Yang, J., Clarke, J., Stirparo, G.G., von Meyenn, F., Dietmann, S., Baker, D., Drummond, R., Ren, Y., Li, D., et al. (2019). Wnt inhibition facilitates RNA-mediated reprogramming of human somatic cells to naive pluripotency. Stem Cell Reports *13*, 1083–1098.

Brons, I.G., Smithers, L.E., Trotter, M.W., Rugg-Gunn, P., Sun, B., Chuva de Sousa Lopes, S.M., Howlett, S.K., Clarkson, A., Ahrlund-Richter, L., Pedersen, R.A., et al. (2007). Derivation of pluripotent epiblast stem cells from mammalian embryos. Nature *448*, 191–195.

Bryant, D.M., and Mostov, K.E. (2008). From cells to organs: building polarized tissue. Nat. Rev. Mol. Cell Biol. *9*, 887–901.

Bryant, D.M., Roignot, J., Datta, A., Overeem, A.W., Kim, M., Yu, W., Peng, X., Eastburn, D.J., Ewald, A.J., Werb, Z., et al. (2014). A molecular switch for the orientation of epithelial cell polarization. Dev. Cell *31*, 171–187.

Chen, G., Hou, Z., Gulbranson, D.R., and Thomson, J.A. (2010). Actin-myosin contractility is responsible for the reduced viability of dissociated human embryonic stem cells. Cell Stem Cell *7*, 240–248.

Chen, G., Gulbranson, D.R., Hou, Z., Bolin, J.M., Ruotti, V., Probasco, M.D., Smuga-Otto, K., Howden, S.E., Diol, N.R., Propson, N.E., et al. (2011). Chemically defined conditions for human iPSC derivation and culture. Nat. Methods. *8*, 424–429.

Clevers, H. (2016). Modeling development and disease with organoids. Cell *165*, 1586–1597.

Deglincerti, A., Croft, G.F., Pietila, L.N., Zernicka-Goetz, M., Siggia, E.D., and Brivanlou, A.H. (2016). Self-organization of the in vitro attached human embryo. Nature *533*, 251–254.

Dong, C., Beltcheva, M., Gontarz, P., Zhang, B., Popli, P., Fischer, L.A., Khan, S.A., Park, K.M., Yoon, E.J., Xing, X., et al. (2020). Derivation of trophoblast stem cells from naïve human pluripotent stem cells. eLife *9*, e52504.

Enders, A.C., Schlafke, S., and Hendrickx, A.G. (1986). Differentiation of the embryonic disc, amnion, and yolk sac in the rhesus monkey. Am. J. Anat. *177*, 161–185.

Fischlechner, M., Schaerli, Y., Mohamed, M.F., Patil, S., Abell, C., and Hollfelder, F. (2014). Evolution of enzyme catalysts caged in biomimetic gel-shell beads. Nat. Chem. *6*, 791–796.

Gao, L., Nath, S.C., Jiao, X., Zhou, R., Nishikawa, S., Krawetz, R., Li, X., and Rancourt, D.E. (2019). Post-passage rock inhibition induces cytoskeletal aberrations and apoptosis in human embryonic stem cells. Stem Cell Res. *41*, 101641.

Guo, G., von Meyenn, F., Rostovskaya, M., Clarke, J., Dietmann, S., Baker, D., Sahakyan, A., Myers, S., Bertone, P., Reik, W., et al. (2017). Epigenetic resetting of human pluripotency. Dev *144*, 2748–2763.

Guo, G., Stirparo, G.G., Strawbridge, S., Yang, J., Clarke, J., Li, M.A., Myers, S., Özel, B.N., Nichols, J., and Smith, A. (2020). Trophectoderm potency is retained exclusively in human naïve cells. BioRxiv https://doi.org/10.1101/2020.02.04.933812.

Hertig, A.T., Rock, J., and Adams, E.C. (1956). A description of 34 human ova within the first 17 days of development. Am. J. Anat. *98*, 435–493.

Huebner, A., Srisa-Art, M., Holt, D., Abell, C., Hollfelder, F., DeMello, A.J., and Edel, J.B. (2007). Quantitative detection of protein expression in single cells using droplet microfluidics. Chem. Commun. *2007*, 1218–1220.

Huebner, A., Sharma, S., Srisa-Art, M., Hollfelder, F., Edel, J.B., and DeMello, A.J. (2008). Microdroplets: a sea of applications? Lab. Chip *8*, 1244–1254.

International Stem Cell, I., Adewumi, O., Aflatoonian, B., Ahrlund-Richter, L., Amit, M., Andrews, P.W., Beighton, G., Bello, P.A., Benvenisty, N., Berry, L.S., et al. (2007). Characterization of human embryonic stem cell lines by the International Stem Cell Initiative. Nat. Biotechnol. *25*, 803–816.

Kleine-Brüggeney, H., van Vliet, L.D., Mulas, C., Gielen, F., Agley, C.C., Silva, J.C.R., Smith, A., Chalut, K., and Hollfelder, F. (2019). Long-term perfusion culture of monoclonal embryonic stem cells in 3D hydrogel beads for continuous optical analysis of differentiation. Small *15*, 1804576.

Kleinman, H.K., and Martin, G.R. (2005). Matrigel: basement membrane matrix with biological activity. Semin. Cancer Biol. *15*, 378–386.

Krtolica, A., Genbacev, O., Escobedo, C., Zdravkovic, T., Nordstrom, A., Vabuena, D., Nath, A., Simon, C., Mostov, K., and Fisher, S.J. (2007). Disruption of apical-basal polarity of human embryonic stem cells enhances hematoendothelial differentiation. Stem Cells *25*, 2215–2223.

Luckett, W.P. (1978). Origin and differentiation of the yolk sac and extraembryonic mesoderm in presomite human and rhesus monkey embryos. Am. J. Anat. *152*, 59–97.

Martyn, I., Brivanlou, A.H., and Siggia, E.D. (2019). A wave of WNT signaling balanced by secreted inhibitors controls primitive streak formation in micropattern colonies of human embryonic stem cells. Development *146*, dev172791.

Moris, N., Anlas, K., van den Brink, S.C., Alemany, A., Schröder, J., Ghimire, S., Balayo, T., van Oudenaarden, A., and Martinez Arias, A. (2020). An in vitro model of early anteroposterior organization during human development. Nature *582*, 410–415.

Mulas, C., Hodgson, A.C., Kohler, T.N., Agley, C.C., Humphreys, P., Kleine-Brüggeney, H., Hollfelder, F., Smith, A., and Chalut, K.J. (2020). Microfluidic platform for 3D cell culture with live imaging and clone retrieval. Lab. Chip *20*, 2580–2591.

Nakamura, T., Okamoto, I., Sasaki, K., Yabuta, Y., Iwatani, C., Tsuchiya, H., Seita, Y., Nakamura, S., Yamamoto, T., and Saitou, M. (2016). A developmental coordinate of pluripotency among mice, monkeys and humans. Nature *537*, 57–62.

Nichols, J., and Smith, A. (2009). Naive and primed pluripotent states. Cell Stem Cell *4*, 487–492.

O'Brien, L.E., Jou, T.S., Pollack, A.L., Zhang, Q., Hansen, S.H., Yurchenco, P., and Mostov, K.E. (2001). Rac1 orientates epithelial apical polarity through effects on basolateral laminin assembly. Nat. Cell Biol. *3*, 831–838.

Ohgushi, M., Matsumura, M., Eiraku, M., Murakami, K., Aramaki, T., Nishiyama, A., Muguruma, K., Nakano, T., Suga, H., Ueno, M., et al. (2010). Molecular pathway and cell state responsible for dissociation-induced apoptosis in human pluripotent stem cells. Cell Stem Cell *7*, 225–239.

Pastor, W.A., Liu, W., Chen, D., Ho, J., Kim, R., Hunt, T.J., Lukianchikov, A., Liu, X., Polo, J.M., Jacobsen, S.E., et al. (2018). TFAP2C regulates transcription in human naive pluripotency by opening enhancers. Nat. Cell Biol. *20*, 553–564.

Rock, J., and Hertig, A.T. (1948). The human conceptus during the first two weeks of gestation. Am. J. Obstet. Gynecol. *55*, 6–17.

Ross, C., and Boroviak, T.E. (2020). Origin and function of the yolk sac in primate embryogenesis. Nat. Commun. *11*, 3760.

Rossant, J., and Tam, P.P.L. (2018). Exploring early human embryo development. Science *360*, 1075–1076.

Sasaki, K., Nakamura, T., Okamoto, I., Yabuta, Y., Iwatani, C., Tsuchiya, H., Seita, Y., Nakamura, S., Shiraki, N., Takakuwa, T., et al. (2016). The germ cell fate of cynomolgus monkeys is specified in the nascent amnion. Dev. Cell *39*, 169–185.

Shahbazi, M.N., Jedrusik, A., Vuoristo, S., Recher, G., Hupalowska, A., Bolton, V., Fogarty, N.M.E., Campbell, A., Devito, L.G., Ilic, D., et al. (2016). Self-organization of the human embryo in the absence of maternal tissues. Nat. Cell Biol. *18*, 700–708.

Shahbazi, M.N., Scialdone, A., Skorupska, N., Weberling, A., Recher, G., Zhu, M., Jedrusik, A., Devito, L.G., Noli, L., MacAulay, I.C., et al. (2017). Pluripotent state transitions coordinate morphogenesis in mouse and human embryos. Nature *552*, 239–243.

Shao, Y., Taniguchi, K., Townshend, R.F., Miki, T., Gumucio, D.L., and Fu, J. (2017a). A pluripotent stem cell-based model for post-implantation human amniotic sac development. Nat. Commun. *8*, 208.

Shao, Y., Taniguchi, K., Gurdziel, K., Townshend, R.F., Xue, X., Yong, K.M.A., Sang, J., Spence, J.R., Gumucio, D.L., and Fu, J. (2017b). Self-organized amniogenesis by human pluripotent stem cells in a biomimetic implantation-like niche. Nat. Mater. *16*, 419–425.

Simunovic, M., Metzger, J.J., Etoc, F., Yoney, A., Ruzo, A., Martyn, I., Croft, G., You, D.S., Brivanlou, A.H., and Siggia, E.D. (2019). A 3D model of a human epiblast reveals BMP4-driven symmetry breaking. Nat. Cell Biol. *21*, 900–912.

Srinivasan, S., Ashok, V., Mohanty, S., Das, A., Das, S., Kumar, S., Sen, S., and Purwar, R. (2017). Blockade of Rho-associated protein kinase (ROCK) inhibits the contractility and invasion potential of cancer stem like cells. Oncotarget *8*, 21418–21428.

Stirparo, G.G., Boroviak, T., Guo, G., Nichols, J., Smith, A., and Bertone, P. (2018). Integrated analysis of single-cell embryo data yields a unified transcriptome signature for the human pre-implantation epiblast. Development *145*, dev158501.

Takashima, Y., Guo, G., Loos, R., Nichols, J., Ficz, G., Krueger, F., Oxley, D., Santos, F., Clarke, J., Mansfield, W., et al. (2014). Resetting transcription factor control circuitry toward ground-state pluripotency in human. Cell *158*, 1254–1269.

Taniguchi, K., Shao, Y., Townshend, R.F., Tsai, Y.H., Delong, C.J., Lopez, S.A., Gayen, S., Freddo, A.M., Chue, D.J., Thomas, D.J., et al. (2015). Lumen formation is an intrinsic property of isolated human pluripotent stem cells. Stem Cell Reports *5*, 954–962.

Taniguchi, K., Shao, Y., Townshend, R.F., Cortez, C.L., Harris, C.E., Meshinchi, S., Kalantry, S., Fu, J., O'Shea, K.S., and Gumucio, D.L. (2017). An apicosome initiates self-organizing morphogenesis of human pluripotent stem cells. J. Cell Biol. *216*, 3981–3990.

Tesar, P.J., Chenoweth, J.G., Brook, F.A., Davies, T.J., Evans, E.P., Mack, D.L., Gardner, R.L., and McKay, R.D. (2007). New cell lines from mouse epiblast share defining features with human embryonic stem cells. Nature *448*, 196–199.

Theberge, A.B., Courtois, F., Schaerli, Y., Fischlechner, M., Abell, C., Hollfelder, F., and Huck, W.T.S. (2010). Microdroplets in microfluidics: an evolving platform for discoveries in chemistry and biology. Angew. Chem. Int. Ed. *49*, 5846–5868.

Theunissen, T.W., Powell, B.E., Wang, H., Mitalipova, M., Faddah, D.A., Reddy, J., Fan, Z.P., Maetzel, D., Ganz, K., Shi, L., et al. (2014). Systematic identification of culture conditions for induction and maintenance of naive human pluripotency. Cell Stem Cell *15*, 471–487.

Tokuoka, Y., Yamada, T.G., Mashiko, D., Ikeda, Z., Hiroi, N.F., Kobayashi, T.J., Yamagata, K., and Funahashi, A. (2020). 3D convolutional neural networks-based segmentation to acquire quantitative criteria of the nucleus during mouse embryogenesis. Npj Syst. Biol. Appl. *6*, 32.

Tyser, R.C.V., Mahammadov, E., Nakanoh, S., Vallier, L., Scialdone, A., and Srinivas, S. (2020). A spatially resolved single cell atlas of human gastrulation. BioRxiv. https://doi.org/10.1101/2020.07.21.213512.

Vernardis, S.I., Terzoudis, K., Panoskaltsis, N., and Mantalaris, A. (2017). Human embryonic and induced pluripotent stem cells maintain phenotype but alter their metabolism after exposure to ROCK inhibitor. Sci. Rep. *7*, 42138.

Warmflash, A., Sorre, B., Etoc, F., Siggia, E.D., and Brivanlou, A.H. (2014). A method to recapitulate early embryonic spatial patterning in human embryonic stem cells. Nat. Methods *11*, 847–854.

Watanabe, K., Ueno, M., Kamiya, D., Nishiyama, A., Matsumura, M., Wataya, T., Takahashi, J.B., Nishikawa, S., Nishikawa, S., Muguruma, K., et al. (2007). A ROCK inhibitor permits survival of dissociated human embryonic stem cells. Nat. Biotechnol. *25*, 681–686.

Xiang, L., Yin, Y., Zheng, Y., Ma, Y., Li, Y., Zhao, Z., Guo, J., Ai, Z., Niu, Y., Duan, K., et al. (2020). A developmental landscape of 3D-cultured human pre-gastrulation embryos. Nature *577*, 537–542.

Ying, Q.L., Wray, J., Nichols, J., Batlle-Morera, L., Doble, B., Woodgett, J., Cohen, P., and Smith, A. (2008). The ground state of embryonic stem cell self-renewal. Nature *453*, 519–523.

Yu, L., Wei, Y., Duan, J., Schmitz, D.A., Sakurai, M., Wang, L., Wang, K., Zhao, S., Hon, G.C., and Wu, J. (2021). Blastocyst-like structures generated from human pluripotent stem cells. Nature *591*, 620–626.

Yu, W., Shewan, A.M., Brakeman, P., Eastburn, D.J., Datta, A., Bryant, D.M., Fan, Q.W., Weiss, W.A., Zegers, M.M.P., and Mostov, K.E. (2008). Involvement of RhoA, ROCK I and myosin II in inverted orientation of epithelial polarity. EMBO Rep. *9*, 923–929.

Zheng, Y., Xue, X., Shao, Y., Wang, S., Esfahani, S.N., Li, Z., Muncie, J.M., Lakins, J.N., Weaver, V.M., Gumucio, D.L., et al. (2019). Controlled modelling of human epiblast and amnion development using stem cells. Nature *573*, 421–425.